AIP | Journal of Applied Physics

First principles study of the interface between silicone and undoped/doped BaTiO3

G. Pilania, K. Slenes, and R. Ramprasad

Citation: J. Appl. Phys. 113, 064316 (2013); doi: 10.1063/1.4791755
View online: http://dx.doi.org/10.1063/1.4791755
View Table of Contents: http://jap.aip.org/resource/1/JAPIAU/v113/i6
Published by the American Institute of Physics.

First principles study of the interface between silicone and undoped/doped $BaTiO_3$

G. Pilania,[1] K. Slenes,[2] and R. Ramprasad[1,a)]
[1]*Materials Science and Engineering, Institute of Materials Science, University of Connecticut, Storrs, Connecticut 06269, USA*
[2]*TPL, Inc., 3921 Academy Parkway North, NE, Albuquerque, New Mexico 87109, USA*

(Received 20 September 2012; accepted 28 January 2013; published online 14 February 2013)

We investigate the local electronic structure and the surface adhesion strength of a silicone-$BaTiO_3$ (001) interface through first principles density functional theory (DFT) computations. A polydimethyl siloxane (PDMS) chain was used as a representative siloxane, and the adsorption of PDMS on both undoped as well as *n*-type (La at Ba site) and *p*-type (Mn at Ti site) doped $BaTiO_3$ (001) surfaces are considered. Our interface is modeled in a two dimensional periodical slab model framework and both the possible $BaTiO_3$ (001) surface terminations (i.e., the BaO- and TiO_2-terminations) are explicitly taken into account. Our calculations indicate that while both *n*-type and *p*-type dopants are expected to improve adhesion of silicone chains at the $BaTiO_3$ surfaces, the *n*-type doping is expected to result in an interface with a clean band gap and superior effective dielectric properties. *p*-type doping could lead to a metallic behavior in the near-interface regions through introduction of mostly unoccupied mid-gap states. Finally, the silicone bonding induced electronic perturbation on both the doped (001) facets of $BaTiO_3$ is analyzed using charge density redistribution analysis. © *2013 American Institute of Physics*. [http://dx.doi.org/10.1063/1.4791755]

I. INTRODUCTION

Recently, inorganic-organic hybrid nanocomposite materials have attracted much scientific and technological interest owing to their potential for use in high energy density storage applications. By integrating the complementary properties of their constituents, these materials can simultaneously provide high dielectric permittivity (arising from the well dispersed inorganic inclusions) as well as properties such as high breakdown strength, mechanical flexibility and processability (contributed by the organic polymer host matrix).[1,2] Furthermore, sufficient theoretical evidence is also available in the literature suggesting that large inclusion-matrix interfacial areas are capable of providing enhanced polarization, dielectric response, and breakdown strength.[3–5]

Several synthetic routes such as mechanical blending,[6] solution mixing,[7–11] *in-situ* nanoparticle synthesis,[12,13] and *in-situ* radical polymerization[14–16] are available to create inorganic-polymer hybrid nanocomposites. However, nanoparticle aggregation and phase separation in the polymer matrix over large length scales frequently occur during the course of synthesis,[17,18] eventually leading to degraded electrical properties of the hybrid composite.[19,20] Therefore, in order to prevent the agglomeration and stabilize the dispersion of ceramic inclusions in an organic host, as-received ceramic particles are surface modified prior to their suspension in the organic monomer.

Poly(dimethyl siloxane) (PDMS)[21,22] is a simple yet one of the most widely used silicone which is frequently employed for the surface pretreatment of ceramic inclusions. Owing to its unique surface properties such as strong hydrophobic nature,[23,24] zero shear viscosity and stability over a wide range of temperatures, PDMS finds applications in diverse fields of biomedical, semiconductor and automobile industry.[25–28] The flexible Si-O backbone together with the low intermolecular interaction of the methyl groups impart PDMS a soft but stable surface with relatively low surface tension.

While many experimental and theoretical studies targeted to understand electronic and dielectric properties of $BaTiO_3$[29–36] and organic polymers[37,38] exist in the literature, investigations targeted to understand the electronic structure of $BaTiO_3$-silicone interface have been very scarce. In this contribution, we focus on local electronic structure and the surface adhesion strength of silicone-$BaTiO_3$ (001) interface through first principles based density functional theory (DFT) computations.[39,40]

The remainder of this paper is organized as follows. In Sec. II, we provide details concerning the model and the computational methodology used. Our results for the undoped and doped interfaces are discussed in Secs. III A and III B, respectively. Finally, our conclusions are summarized in Sec. IV.

II. METHODOLOGY DETAILS

Our calculations were carried out using DFT[39,40] as implemented in the Vienna *Ab initio* Simulation Package (VASP)[41,42] with the electronic wave functions expanded in a plane wave basis with a cutoff energy of 400 eV. The generalized gradient approximation (GGA)[43,44] with projector augmented wave (PAW)[45,46] method was used. The atomic positions were relaxed until the maximum component of the force on any atom was smaller than 0.02 eV/Å. Monkhorst-Pack *k*-point mesh[47] of $8 \times 8 \times 8$ was used to produce well converged results with (1×1) bulk unit cells, respectively.

a)Electronic address: rampi@ims.uconn.edu.

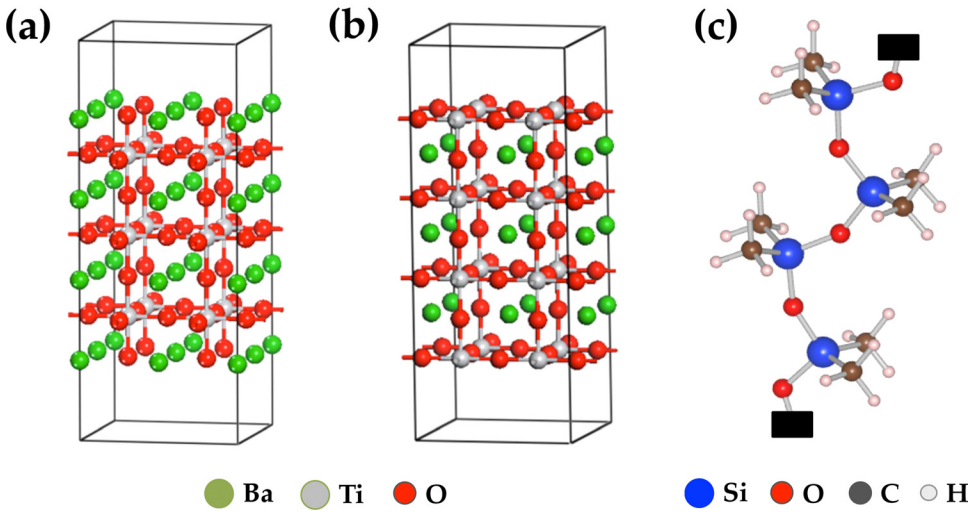

FIG. 1. Atomistic models of seven layer thick (a) BaO- and (b) TiO_2-terminated (001) $BaTiO_3$ surface facets in a symmetric slab geometry and (c) polydimethyl siloxane (a model linear silicone) chain segment that were used further to simulate $BaTiO_3$-silicone interface in the present study. The binding sites on the silicone chain are identified using black rectangles.

Within the above approximations, the calculated $BaTiO_3$ bulk lattice constant in the cubic phase is predicted to be 4.03 Å, in good agreement with prior experimental[48,49] and theoretical[50] results. This calculated bulk lattice constant was then further used to construct the clean surfaces and the interface models. Before moving onto interface models, the clean BaO- and TiO_2-terminated surfaces were first modeled in a symmetric slab geometry configuration (to avoid any artificial dipole moment along the surface normal) with a mirror plane passing through the center of the slab. As shown in Figures 1(a) and 1(b), Each of the slabs was 7 layers thick with central three layers were fixed at the bulk lattice constant to have bulk like behavior in the interior of the slab. A Monkhorst-Pack k-point mesh of $8 \times 8 \times 1$ was employed to model the two surface facets with (1×1) surface supercell. The calculated average surface energy, surface rumpling and surface relaxations for the two surface terminations were found to be in agreement with other previous studies available in the literature.[35,36]

To model the aspired interface structures, PDMS was used as a model silicone (c.f. Fig. 1(c)). A (2×2) surface supercell, with one out of the four surface metal ions passivated by polydimethyl siloxane, was used to model the undoped $BaTiO_3$-silicone interface. In both the interface models, the oxygen atom in the silicone chain binds to the surface metal ion. For the doped interface, La-doped BaO-terminated and Mn-doped TiO_2-terminated (001) $BaTiO_3$ surfaces were used to simulate n-type and p-type doping situations, respectively. Furthermore, two different surface locations for the dopant atoms were considered for each of the n-type and p-type doped interfaces: directly bound to the silicone chain and at a neighboring site to the silicone chain. Each of the undoped and doped interfaces was fully relaxed using the procedure described above for the clean $BaTiO_3$ surfaces.

III. RESULTS

A. Undoped interfaces

To access the relative stability of the silicone-$BaTiO_3$ (001) interface and to quantitatively measure the degree of adhesion between the surface and the silicone chain, we considered the reaction enthalpy of the following reaction:

$$\underset{\text{(undoped or doped)}}{\mathbf{BaTiO_3\ surface}} + \underset{\text{(H passivated)}}{\mathbf{Silicone\ chain}} \rightarrow \underset{\text{(interface)}}{\mathbf{Silicone-BaTiO_3}} + \underset{\text{(gas)}}{\mathbf{H_2}} \quad (1)$$

To compute the reaction enthalpy, the required DFT energies of the H-passivated silicone chain and the H_2 molecule were calculated using large supercells that employed a vacuum of at least 12 Å between the periodic images of the molecules, to minimize the unphysical interactions arising due to the periodic boundary conditions. A negative value of the reaction enthalpy (or the binding energy) indicates a thermodynamically stable interface. Our results, presented in Table I, indicate that the both undoped silicone-$BaTiO_3$ (001) (i.e., with the BaO- and TiO_2-terminations) interfaces are thermodynamically unstable with the above reaction being endothermic in nature for both the interfaces.

The relaxed interface models of the (001) $BaTiO_3$ facets with PDMS were next subjected to the layer-decomposed density of states (LaDOS) analysis to assess the local electronic structure across the interface. Within the LaDOS approach, the total density of states (DOS) of the entire system is decomposed in terms of its origins from the various atoms of the system on a layer-by-layer basis. To do this, the wavefunction character is first calculated by projecting the orbitals onto spherical harmonics that are non-zero within spheres of predefined radii around each of the atoms and then the LaDOS is calculated by summing up all the contributions from the atoms constituting a given layer.

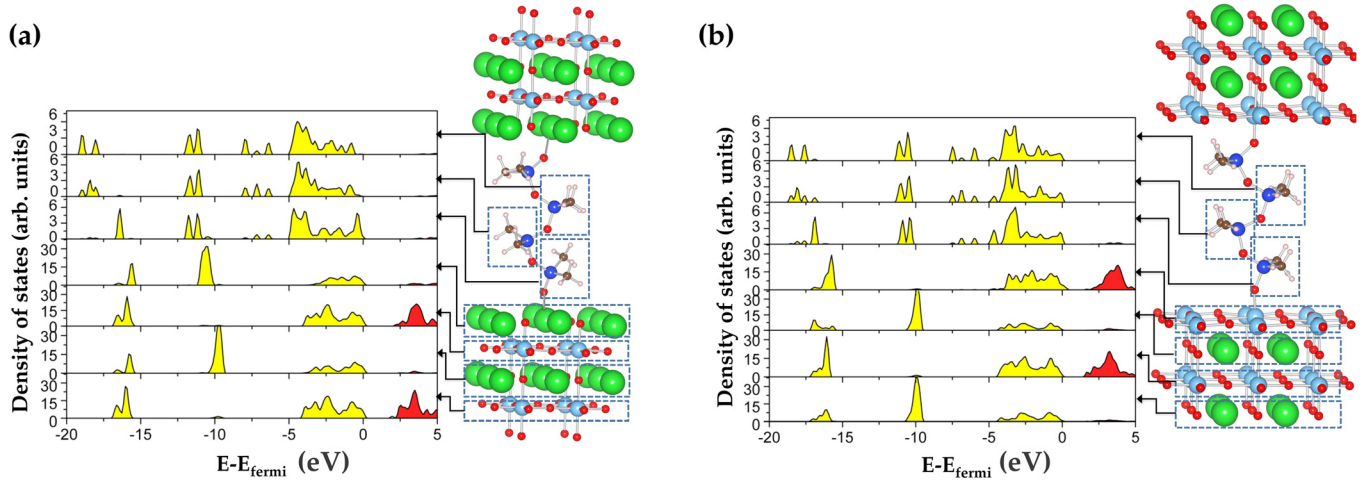

FIG. 2. Calculated layer-decomposed density of states (LaDOS) for the (001) (a) BaO- and (b) TiO_2-terminated undoped $BaTiO_3$-silicone interface. In each of the cases, the occupied and empty states are shown in yellow and red colors, respectively. The relaxed model defining various contributing layers across the interface are also shown on the left in each of the panels.

The calculated LaDOS for the (001) BaO- and TiO_2-terminated undoped $BaTiO_3$-silicone interface is presented in Figures 2(a) and 2(b), respectively. We note that, similar to the $BaTiO_3$ bulk[51] and the two (001) clean surface facets,[52] oxygen *p* orbitals are the primary contributors to the top part of the valence band and the bottom of conduction bands is formed by Ti 3*d* orbitals in the two undoped $BaTiO_3$-silicone interfaces. While the silicone chain mainly contributes to the valence band of the interface, our results indicate that the undoped silicone-$BaTiO_3$ interfaces have a band gap similar to that of the clean surfaces with no mid-gap surface states in the band gap.

B. Doped interfaces

To understand the possible effect of doping on the relative stability of the interface structure in terms of its influence on the local electronic structure, next we consider the doped interfaces. Doping of La at Ba site (*i.e.*, *n*-type doping) and Mn ions at Ti site (i.e., *p*-type doping) in the top interfaces layer was considered. For each of the two doping situations, two different doping configurations namely *underneath* (dopant atom lying directly underneath the silicone chain) and *neighboring* (dopant atom lying at the site adjacent to the surface metal ion bonding to the silicone chain) were studied in our analysis.

As reported in Table I, our results for the reaction enthalpy for Eq. (1) indicate that both *n*-type and *p*-type dopants are expected to improve adhesion of silicone chains at the $BaTiO_3$ surfaces, as compared to the undoped interfaces. While for the La-doped interface silicone chain prefers to bind to the surface La ion, we find that in case of the Mn-doped interface it is energetically more favorable for the silicone to bind to the surface Ti ion in vicinity of the doped Mn atom. The thermodynamic stability of the La-doped interface can further be understood on the basis of simple electron counting notions. The extra electrons donated by La ions (with +3 nominal oxidation state and substituting Ba^{+2} ions) are used towards completing the octet of the surface bonded oxygen atom of the silicone chain.

TABLE I. The calculated binding energies for various interface models investigated in the present study.

Doping type	Termination	Dopant location	Binding energy (eV)
Undoped	BaO	–	2.38
	TiO_2	–	1.54
p-type	BaO	Underneath	−2.59
	BaO	Neighboring	−1.51
n-type	TiO_2	Underneath	−0.21
	TiO_2	Neighboring	−1.19

Our calculated LaDOS for the *n*-type and *p*-type doped $BaTiO_3$-silicone interfaces, for the configuration in which the dopant atom lies directly underneath the silicone chain, are presented in Figures 3(a) and 3(b), respectively. We would also like to mention that the LaDOS profiles for the *n*-type and *p*-type doped $BaTiO_3$-silicone interfaces for the second configuration, in which the dopant atom lies at the neighboring site with respect to the surface metal atom directly bonded to the silicone chain, were found to be qualitatively quite similar to the ones presented in Figure 3 and therefore are not reported here. While La-doping preserves the electronic structure of the $BaTiO_3$ surface, Mn-doping creates plenty of occupied and mostly unoccupied interface states. The surface states appear at the interface (in the Mn-doped TiO_2-layer as well as in the first layer of the silicone chain) in the case of the *p*-doped silicone-$BaTiO_3$ interface, indicating the sensitivity of the electronic structure to the type of doping and the nature of the surface preparation.

To visualize the charge rearrangements upon the silicone adsorption on the two doped interfaces, we further carried out the difference electron density analysis presented in Figure 4. The difference electron density is obtained by subtracting the electron charge density of both an isolated silicone chain and a surface (either La-doped BaO-terminated or Mn-doped TiO_2-terminated $BaTiO_3$ surface) from that of the respective relaxed $BaTiO_3$-silicone interfaces. To highlight only the local rearrangements in the electronic charge

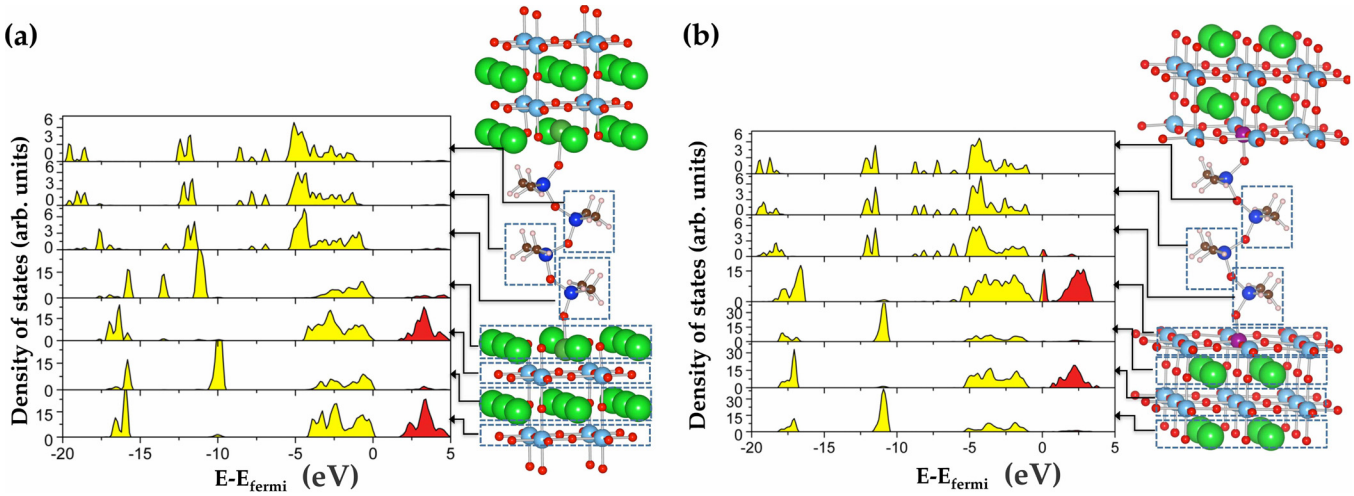

FIG. 3. Calculated layer-decomposed density of states (LaDOS) for the (001) (a) La-doped BaO- and (b) Mn-doped TiO_2-terminated $BaTiO_3$-silicone interface. In each of the cases, the occupied and empty states are shown in yellow and red colors, respectively. The relaxed model defining various contributing layers across the interface are also shown on the left in each of the panels. In each of the two panels, dopant atoms lie directly underneath the silicone chain.

density occurring due to the silicone-surface bonding, the atomic positions of the two doped surfaces and the silicone are taken to be same as those of the relaxed silicone-surface system.

The analysis of the electron density redistribution due to the silicone adsorption for the doped BaO- and TiO_2-terminated (001) surfaces is shown in Figures 4(a) and 4(b), respectively. A clear donation of charge from the surface metal atom to the bonding oxygen of the silicone chain is clearly visible in each of the two cases. We further note that the silicone bonding induced electronic charge redistribution on both of the (001) facets of $BaTiO_3$ is quite locally confined in the vicinity of the interface and the charges on all other atoms, in the interior of the surface as well as on the silicone chain, remain virtually unaffected due to the bonding.

IV. SUMMARY

We have carried out DFT computations to investigate the local electronic structure and the relative interface stability of the undoped as well as the *n*-type and *p*-type doped silicone-$BaTiO_3$ (001) interfaces. In essence, our results indicate that both *n*-type and *p*-type dopants are expected to improve adhesion of silicone chains at the $BaTiO_3$ surfaces. While, the *n*-type doping results in a clean band gap which is qualitatively similar to that of the clean surface and the undoped interface, the *p*-type doping could lead to metallic behavior in the near-interface regions through introduction of mid-gap states and thereby degrading the effective dielectric properties of the overall inorganic-organic hybrid nanocomposite. Based on the charge density redistribution analysis, we also find that the silicone bonding induced electronic charge redistribution on both of the (001) facets of $BaTiO_3$ is quite locally confined in the vicinity of interface, with the charges on all other layers, except the top-most and penultimate layers, remain virtually unaffected due to the bonding.

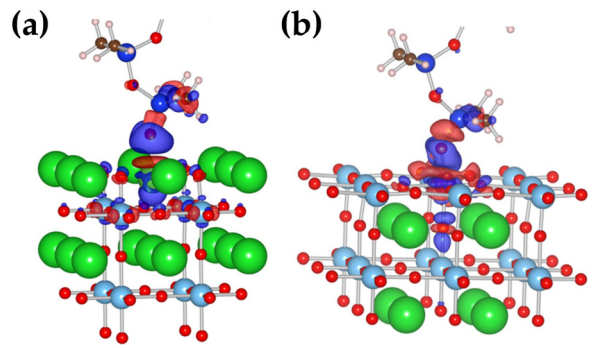

FIG. 4. Difference electron density maps highlighting the electron charge density redistribution due to the silicone adsorption for the (a) La-doped BaO-, (b) Mn-doped TiO_2-terminated (001) $BaTiO_3$ surface. An isosurface corresponding to an electron charge density of 0.02 e/Å^3 is shown in each of the panels. Red and blue colors have been used to represent depletion and accumulation of charge, respectively. The representation of atoms is same as that used in Figure 3.

ACKNOWLEDGMENTS

This material is based upon work supported by an Air Force STTR subcontract from TPL, Inc. Partial computational support through a National Science Foundation Teragrid allocation is also gratefully acknowledged.

[1]T. Tanaka, G. C. Montanari, and R. Mülhaupt, IEEE Trans. Dielectr. Electr. Insul. **11**, 763 (2004).
[2]R. E. Newnham, Annu. Rev. Mater. Sci. **16**, 47 (1986).
[3]S. K. Saha, Phys. Rev. B **69**, 125416 (2004).
[4]J. K. Nelson, L. A. Utracki, R. K. MacCrone, and C. W. Reed, in *2004 Annual Report Conference on Electrical Insulation and Dielectric Phenomena, CEIDP '04* (IEEE, 2004), 314–317.
[5]J. Li, Phys. Rev. Lett. **90**, 217601 (2003).
[6]Z. Dang, J. Wu, L. Fan, and C. Nan, Chem. Phys. Lett. **376**, 389 (2003).
[7]N. Parvatikar and M. V. N. Ambika Prasad, J. Appl. Polym. Sci. **100**, 1403 (2006).
[8]P. Badheka, V. Magadala, N. Gopi Devaraju, B. I. Lee, and E. S. Kim, J. Appl. Polym. Sci. **99**, 2815 (2006).
[9]S. Xie, B. Zhu, Z. Xu, and Y. Xu, Mater. Lett. **59**, 2403 (2005).
[10]R. Schroeder, L. Majewski, and M. Grell, Adv. Mater. **17**, 1535 (2005).
[11]Y. Bai, Z. Cheng, V. Bharti, H. Xu, and Q. Zhang, Appl. Phys. Lett. **76**, 3804 (2000).

[12]J. Lu, K. S. Moon, J. Xu, and C. P. Wong, J. Mater. Chem. **16**, 1543 (2006).
[13]T. Yogo, T. Yamamoto, W. Sakamoto, and S. Hirano, J. Mater. Res. **19**, 3290 (2004).
[14]A. He, L. Wang, J. Li, J. Dong, and C. C. Han, Polymer **47**, 1767 (2006).
[15]V. V. Ginzburg, K. Myers, S. Malowinski, R. Cieslinski, M. Elwell, and M. Bernius, Macromolecules **39**, 3901 (2006).
[16]R. Popielarz, C. K. Chiang, R. Nozaki, and J. Obrzut, Macromolecules **34**, 5910 (2001).
[17]M. E. Mackay, A. Tuteja, P. M. Duxbury, C. J. Hawker, B. Van Horn, Z. Guan, G. Chen, and R. S. Krishnan, Science **311**, 1740 (2006).
[18]Y. Lin, A. Boeker, J. He, K. Sill, H. Xiang, C. Abetz, X. Li, J. Wang, T. Emrick, S. Long, Q. Wang, A. Balazs, and T. P. Russell, Nature **434**, 55 (2005).
[19]G. Chen and A. E. Davies, IEEE Trans. Dielectr. Electr. Insul. **7**, 401 (2000).
[20]M. S. Khalil, IEEE Trans. Dielectr. Electr. Insul. **7**, 261 (2000).
[21]*Polymer Data Handbook*, edited by J. E. Mark (Oxford University Press, New York, 1999).
[22]*Silicon Based Polymers Advances in Synthesis and Supramolecular Organization*, edited by F. Ganachaud, S. Boileau, and B. Boury (Springer, New York, 2008).
[23]M. Ma and R. M. Hill, Curr. Opin. Colloid Interface Sci. **11**, 193 (2006).
[24]P. Roach, N. J. Shirtcliffe, and M. I. Newton, Soft Matter **4**, 224 (2008).
[25]S. J. Clarson and J. A. Semlyen, *Siloxane Polymers* (PTR Prentice-Hall Inc., New Jersey, 1993).
[26]M. Owen, J. Ind. Eng. Chem. Prod. Res. Dev. **19**, 97 (1980).
[27]B. Arkles, Chemtech. **13**, 542 (1983).
[28]J. L. Wilbur, E. Kim, Y. Xia, and G. M. Whitesides, Adv. Mater. **7**, 649 (1995).
[29]S. Roberts, Phys. Rev. **71**, 890 (1947).
[30]G. A. Samara, Phys. Rev. **151**, 378 (1966).
[31]R. E. Cohen, J. Phys. Chem. Solids **57**, 1393 (1996).
[32]R. E. Cohen, Ferroelectrics **194**, 323 (1997).
[33]J. Padilla and D. Vanderbilt, Phys. Rev. B **56**, 1625 (1997).
[34]P. Ghosez, Ph.D. dissertation, Universite Catholique de Louvain, 1977.
[35]B. Meyer, J. Padilla, and D. Vanderbilt, Faraday Discuss **114**, 395 (1999).
[36]B. Meyer and D. Vanderbilt, Phys. Rev. B **63**, 205426 (2001).
[37]R. P. Ortiz, A. Facchetti, and T. J. Marks, Chem. Rev. **110**, 205 (2010).
[38]W. Volksen, R. D. Miller, and G. Dubois, Chem. Rev. **110**, 56 (2010).
[39]P. Hohenberg and W. Kohn, Phys. Rev. **136**, B864 (1964).
[40]W. Kohn and L. Sham, Phys. Rev. **140**, A1133 (1965).
[41]G. Kresse and J. Hafner, Phys. Rev. B **47**, 558 (1993).
[42]G. Kresse and J. Furthmüller, Phys. Rev. B **54**, 11169 (1996).
[43]J. P. Perdew, J. A. Chevary, S. H. Vosko, K. A. Jackson, M. R. Pederson, D. J. Singh, and C. Fiolhais, Phys. Rev. B **46**, 6671 (1992).
[44]J. P. Perdew, J. A. Chevary, S. H. Vosko, K. A. Jackson, M. R. Pederson, D. J. Singh, and C. Fiolhais, Phys. Rev. B **48**, 4978 (1993).
[45]P. E. Blöchl, Phys. Rev. B **50**, 17953 (1994).
[46]G. Kresse and D. Joubert, Phys. Rev. B **59**, 1758 (1999).
[47]H. J. Monkhorst and J. D. Pack, Phys. Rev. B **13**, 5188 (1976).
[48]G. Shirane, H. Danner, and R. Pepinsky, Phys. Rev. **105**, 856 (1957).
[49]*Ferroelectrics and Related Substances*, edited by K. H. Hellwege and A. M. Hellwege, Landolt-Börnstein, New Series, Group III (Springer Verlag, Berlin, 1969), Vol. 3.
[50]S. Sanna, C. Thierfelder, S. Wippermann, T. P. Sinha, and W. G. Schmidt, Phys. Rev. B **83**, 054112 (2011).
[51]S. Piskunov, E. Heifets, R. I. Eglitis, and G. Borstel, Comput. Mater. Sci. **29**, 165 (2004).
[52]S. Piskunov, E. A. Kotomin, and E. Heifets, Microelectron. Eng. **81**, 472 (2005).